Anisotropic atomistic shock response mechanisms of aramid crystals

Emily J. Gurniak, Subodh C. Tiwari, Sungwook Hong, et al.

View Online

Export Citation

CrossMark

Anisotropic atomistic shock response mechanisms of aramid crystals

Emily J. Gurniak,[1] (iD) Subodh C. Tiwari,[2] (iD) Sungwook Hong,[3] (iD) Aiichiro Nakano,[2] (iD) Rajiv K. Kalia,[2] (iD)
Priya Vashishta,[2] (iD) and Paulo S. Branicio[1,a) (iD)

AFFILIATIONS

[1] Department of Chemical Engineering and Materials Science, University of Southern California,
  Los Angeles, California 90089-0242, USA
[2] Collaboratory for Advanced Computing and Simulations, Department of Physics and Astronomy,
  Department of Computer Science, Department of Chemical Engineering and Materials Science,
  Department of Biological Sciences, University of Southern California, Los Angeles, California 90089-0242, USA
[3] Department of Physics and Engineering, California State University, Bakersfield, Bakersfield, California 93311, USA

a) Author to whom correspondence should be addressed: branicio@usc.edu

ABSTRACT

Aramid fibers composed of poly(p-phenylene terephthalamide) (PPTA) polymers are attractive materials due to their high strength, low weight, and high shock resilience. Even though they have widely been utilized as a basic ingredient in Kevlar, Twaron, and other fabrics and applications, their intrinsic behavior under intense shock loading is still to be understood. In this work, we characterize the anisotropic shock response of PPTA crystals by performing reactive molecular dynamics simulations. Results from shock loading along the two perpendicular directions to the polymer backbones, [100] and [010], indicate distinct shock release mechanisms that preserve and destroy the hydrogen bond network. Shocks along the [100] direction for particle velocity $U_p < 2.46$ km/s indicate the formation of a plastic regime composed of shear bands, where the PPTA structure is planarized. Shocks along the [010] direction for particle velocity $U_p < 2.18$ km/s indicate a complex response regime, where elastic compression shifts to amorphization as the shock is intensified. While hydrogen bonds are mostly preserved for shocks along the [100] direction, hydrogen bonds are continuously destroyed with the amorphization of the crystal for shocks along the [010] direction. Decomposition of the polymer chains by cross-linking is triggered at the threshold particle velocity $U_p = 2.18$ km/s for the [010] direction and $U_p = 2.46$ km/s for the [100] direction. These atomistic insights based on large-scale simulations highlight the intricate and anisotropic mechanisms underpinning the shock response of PPTA polymers and are expected to support the enhancement of their applications.

Published under an exclusive license by AIP Publishing. https://doi.org/10.1063/5.0102293

I. INTRODUCTION

Aramid fibers, such as Kevlar and Twaron, are used in a wide assortment of applications, including ballistic armor, cut-resistant gloves, and flame-resistant fabrics, due to their outstanding shock resilience, thermal stability, and strength to weight ratio.[1–8] Investigations of the structure and composition of these fibers suggest that their properties result from domains of poly(p-phenylene terephthalamide) (PPTA) crystals, where the polymer backbones are largely oriented with the fiber axis.[9–12] Traditionally, the development in understanding the relationship between processing conditions, structure, and mechanical properties, necessary

for the improvement of aramid fibers, commonly involves the time-consuming generation of samples and empirical testing of their properties.[13]

Atomistic modeling has been increasingly used to assist in the development and understanding of structure–property relationships in high molecular weight polymers[14–16] and to shed light on important microscopic deformation mechanisms necessary to understand how these materials fail.[17,18] For example, atomistic modeling of polyethylene fibers with chain ends indicates that chain slip is the mechanism defining the tensile yield in these materials.[19] Modeling of PPTA has provided critical data for the development of continuum models of their strength and ductility.[20] Chain-end defects have

also been studied in PPTA via reactive molecular dynamics (MD) simulations that show that load is transferred to adjacent chains during axial loading.[17] These studies highlight the importance of MD simulations to understand the intrinsic deformation mechanisms in polymeric materials.

One particularly insightful application of MD simulations is to describe the shock response of polymers. Atomistic simulations of the shock response of polymers have been performed using quantum mechanical calculations,[21–23] non-reactive force fields,[22,24–26] and reactive force fields.[27,28] In particular, *ab initio* MD studies of PPTA have elucidated the importance of direction-dependent shock-loading mechanisms that preserve or destroy the hydrogen bond network in this material.[21] While these simulations provided important insights into the shock behavior of PPTA, they were restricted to small simulation box sizes due to the high computational cost of *ab initio* calculations. It remains to be determined if the predictions from *ab initio* simulations also apply to large PPTA crystals, representative of realistic aramid fibers' domains. Large PPTA crystal simulation cells are essential to probe distortions that naturally occur on polymer materials at larger length scales[29–31] and to allow for the spontaneous generation of deformation mechanisms that may be constrained by the small simulation cells typically used in *ab initio* simulations.

In this work, we investigate the shock response of PPTA crystals using large-scale reactive MD simulations. We elucidate the anisotropic shock response of PPTA in a wide range of shock velocities from weak elastic/plastic to strong cross-linking regimes. The results contrast with the predictions of previous *ab initio* calculations and highlight the need for a large-scale description of the shock response of complex molecular crystals, such as PPTA.

II. COMPUTATIONAL METHODS

Simulations are performed using the Large-scale Atomic/Molecular Massively Parallel Simulator (LAMMPS) package using real units.[32] Periodic boundary conditions are used in all simulations. The simulation cell is prepared by replicating a PPTA unit cell by $36 \times 20 \times 1$ times to dimensions $283.32 \times 103.6 \times 12.9$ Å^3 for shock simulations along the [100] direction (x-direction) and by $12 \times 60 \times 1$ times to dimensions $94.44 \times 310.8 \times 12.9$ Å^3 for shock simulations along the [010] direction (y-direction). In both systems, the simulation cell contains 40 320 atoms. A subset of the full simulation cell is shown in Fig. 1, with the unit cell structure constructed from x-ray diffraction data.[33] Based on this experimental structural data, we assume an orthorhombic simulation box for all simulations. Thermalized simulation cells show near zero shear stress, indicating that the system is fully equilibrated with an orthorhombic box. PPTA shows a bonding hierarchy along the low-index crystallographic directions. The polymer backbones, aligned along the [001] direction, display strong covalent bonds, as shown in Figs. 1(a) and 1(c). In contrast, along the [010] direction, PPTA sheets are bonded by weaker interactions coming from hydrogen bonds that occur among the donor (nitrogen), hydrogen, and the acceptor (oxygen), as shown in Fig. 1(c). PPTA sheets are bonded along the [100] direction by van der Waals interactions, as shown in Fig. 1(b), which are the weakest of all interactions present.
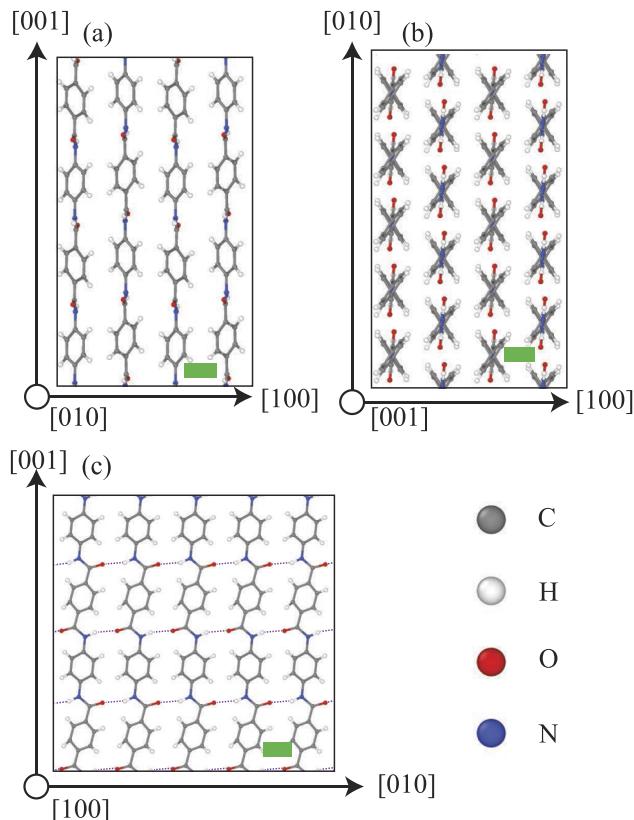

FIG. 1. Structure of the PPTA crystal with views from (a) [010], (b) [001], and (c) [100] directions. Scale bar dimension in (a)–(c) is 2.5 Å. Hydrogen bonds are indicated by dotted lines. (a)–(c) Produced with OVITO version 5.3.3.

Interatomic forces are calculated based on a reactive force field, ReaxFF,[34] which is fine-tuned to the lattice parameters and properties of PPTA crystals. Full details of the ReaxFF parameters used in current simulations and the data used in the fitting are provided in the supplementary material. For pre-shock simulations, a dynamic time step is used with no minimum value and a maximum value of 0.1 fs. The dynamic time step is calculated on the fly by LAMMPS to ensure a maximum atomic displacement of 0.007 Å per time step. Initially, the structure and the simulation box are relaxed by performing a conjugate gradient optimization at zero external pressure. The system is, then, thermalized at 10 K for 10 ps in the isobaric–isothermal ensemble (NPT), which is followed by NPT thermalization at 300 K for another 10 ps.

The Multi-Scale Shock Technique (MSST)[35] is used to generate the shock state for shock waves in the range from 3.2 to 10.0 km/s along the [010] direction and from 4.0 to 10.0 km/s along the [100] direction. In the MSST technique, a shock wave velocity is set and the particle velocity is calculated. In each direction, the minimum shock wave speed is the speed of sound along that direction. Choosing shock wave velocities above this threshold ensures that the simulation converges. Time steps between 0.03 and 0.07 fs are chosen for each simulation to get an accurate atomic trajectory based

on preliminary simulations using dynamic time steps. Equations of motion are integrated up to 63 ps to generate the equilibrium shock state. Table S1 in the supplementary material shows the simulation time steps and total simulation time for each system.

Atomic visualizations and analyses are performed using the Open Visualization Tool, OVITO package.[36] The center of mass of molecules used in the analysis of deformation and amorphization of the systems is calculated using the cluster analysis tool in OVITO. Hydrogen bonds are calculated by considering sets of N, H, O, and C atoms such that (1) the distance between the donor (N) and the acceptor (O) is less than 3.5 Å, (2) the distance between O and H is less than 2.7 Å, (3) the angle formed by the vectors connecting H to N and H to O is greater than 90°, and (4) the angle formed by the vectors connecting O to C and O to H is also greater than 90°.[37–39] Any hydrogen bond not satisfying these four criteria is considered broken. The fraction of sp^2 carbon is evaluated using the coordination number calculated for every carbon atom considering bond cutoff lengths, i.e., C–C 1.7 Å, C–N 1.7 Å, C–O 1.5 Å, and C–H 1.3 Å.

III. RESULTS

To investigate the shock performance of PPTA crystals, we perform MD simulations of shock compression using the MSST method along two crystallographic directions, [100] and [010]. PPTA crystal bonding hierarchy is expected to generate a highly anisotropic shock response along these directions, considering that PPTA sheets interact by weak van der Waals interactions along the [100] direction and hydrogen bonding interaction is prevalent along the [010] direction. The choice of these two shock loading directions is motivated by the application of aramid fibers in composites. Typically, polymer fiber-reinforced composites are designed to maximize the fiber reinforcement, which occurs when the fiber axis is under tensile loading or when compression is applied perpendicular to the fiber axis.[40]

We start by investigating the shock performance along the [010] direction, probing the resistance of the hydrogen bonding network to shocks of different intensities. We perform MSST shock simulations by setting the shock velocity, U_s, which enables the calculation of the particle velocity, U_p. We set the value of U_s in the range from 3.2 to 10.0 km/s, extending all shock intensities. From the calculated U_p values from each simulation, we compile the shock Hugoniot curve shown in Fig. 2(a). From our analysis of the simulation data, we identify three distinct shock response regimes along the [010] direction: elastic/plastic, amorphization, and cross-linking. The three regimes are denoted by different colors, as indicated in Fig. 2(a). The elastic/plastic regime is characterized by systems in which there exists localized plastic deformation or localized amorphization. The amorphization regime is distinguished from the elastic/plastic regime by the presence of plastic or amorphization regions that traverse the entire simulation box. The cross-linking regime denotes systems in which at least one cross-link bond is formed between adjacent polymer chains. There is a gap between the elastic/plastic and amorphization regimes because the MSST method describes a single shock state. This gap indicates that above the last point in the elastic/plastic regime, the elastic/plastic and amorphization waves would coexist.

For weak shocks along the [010] direction, an elastic/plastic response regime is observed. This regime spans from low values of U_p to U_p = 0.235 km/s (U_s = 4.0 km/s), which is depicted by red circles in the shock Hugoniot curve shown in Fig. 2(a). To characterize the changes in the arrangement of the polymer chains in the system, we visualize the simulation cells in this regime. Figures 2(b) and 2(c) illustrate the state of the system in the elastic–plastic regime at U_p = 0.119 km/s. We can see that in this regime, most of the PPTA crystal is elastically compressed along the [010] direction, with no significant changes to its structure. However, localized regions can be observed in the simulation cells, which display irreversible deformation in the form of molecule rotation and changes in the angle between phenylene rings and collective shear flow along the [100] direction. Figure 2(c) shows two zoomed-in regions, highlighting the elastic and plastic regions. This result highlights the fragility of the hydrogen bond network in PPTA crystals to shocks along the [010] direction, which is readily ruptured to release the shear stress generated by shock loading.

With the increase in shock intensity along the [010] direction, the plastic deformation regions, which are spatially localized in the elastic/plastic regime, swiftly increase in volume until they trigger the rupture of hydrogen bonds in most of the simulation cells. This phenomenon occurs from U_p = 0.697 km/s (U_s = 4.4 km/s) and characterizes what we call the amorphization regime, where the crystal arrangement is destroyed with the widespread rupture of hydrogen bonding. At the onset of this regime, an amorphous phase nucleates and coexists in equilibrium with crystalline domains. As the shock intensifies, a uniform amorphous phase develops and occupies the entire simulation cell, as shown in Fig. 2(d), which illustrates the system at U_p = 1.75 km/s (U_s = 6.4 km/s). During the amorphization process, several structural change mechanisms are activated, including molecule rotations, translations, and changes in the angle between phenylene rings, leading to the appearance of planar molecule configurations. The random rotations and translations rupture the hydrogen bonds and disrupt the crystalline arrangement of the molecules, leading to the formation of an amorphous structure. These atomic-level structural changes are illustrated in the visualization shown in Fig. 2(e).

The stability of the hydrogen bond network in the elastic/plastic regime contrasts with that of the amorphization regime. To further quantify this contrast, we evaluate the number of hydrogen bonds in the PPTA systems in the energy minimized, thermalized, and shocked states. In the perfect PPTA crystal, i.e., in the system with the structure relaxed at T = 0 K and P = 0 GPa, the system is saturated with hydrogen bonds as each amide group forms a bond with the adjacent chain. Thermalization of the crystal at 300 K provides sufficient thermal fluctuation that enables rotation of the amide groups to rupture about 10% of the relaxed crystal hydrogen bonds. To evaluate the stability of the hydrogen bonding under shock loading, we calculate the number of hydrogen bonds in the shocked state and normalize it using the reference number of bonds in the crystal relaxed at 0 K. The results are displayed in Fig. 3 and highlight the contrast in the stability of the hydrogen bonds in the elastic/plastic and amorphization states. For weak shocks in the elastic/plastic regime, the structural changes in the plastic regions are largely characterized by collective displacements and rotations, as shown in Figs. 2(b) and 2(c). The shock compression in these systems results in the recovery of a fraction of the hydrogen bonds
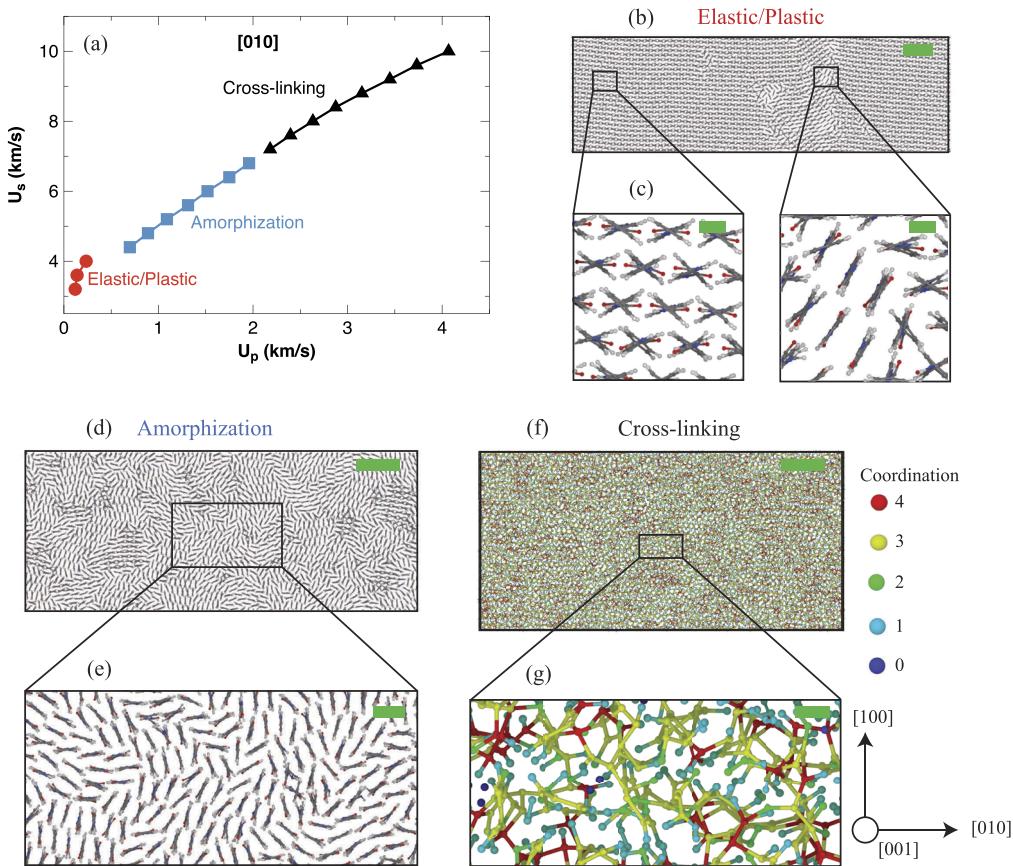
FIG. 2. PPTA [010] shock response regimes. (a) Shock Hugoniot. (b) System at the elastic shock regime at $U_p = 0.12$ km/s with (c) the inset showing a zoomed-in region. (d) System displaying the plastic response for $U_p = 1.75$ km/s with (e) the respective zoomed-in region. (f) System at the crosslinking regime for $U_p = 4.07$ km/s with (g) the zoomed-in region showing increased coordination. (f) and (g) The polymer backbone colored by coordination from 0 (dark blue) to 4 (red). (b)–(e) Colored by atom type based on the scheme used in Fig. 1. Scale bar dimensions: (b) 25 Å, (c) 2.5 Å, (d) 25 Å, (e) 5 Å, (f) 25 Å, and (g) 2 Å. (b)–(g) Produced with OVITO version 5.3.3.
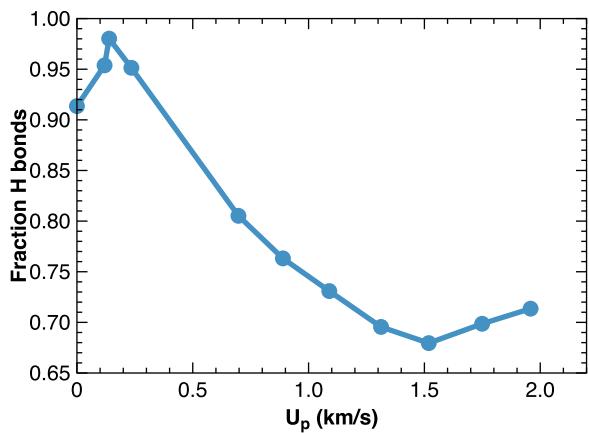

FIG. 3. Fraction of hydrogen bonds as a function of particle velocity for shocks along the [010] direction. The reference for the calculation is the PPTA crystal at 0 K. The value at $U_p = 0.0$ km/s is calculated from the crystal thermalized at 300 K.

lost in the thermalization, indicated by the increasing fraction compared to $U_p = 0.0$ km/s (300 K thermalized crystal) in Fig. 3. In contrast, the rotations and translations that occur in the amorphization shock regime become progressively random as the intensity is increased, as illustrated in Figs. 2(d) and 2(e). As the particle velocity is increased in this regime, the randomness of the chain rotations also increases, disrupting progressively the hydrogen bonds in the process, as quantified in Fig. 3.

The amorphization regime persists in a wide range of shock intensities up to $U_p = 1.96$ km/s ($U_s = 6.8$ km/s). Starting at $U_p = 2.18$ km/s, the system is highly compressed such that the distance between the polymer backbone (carbon, nitrogen, and oxygen) atoms in adjacent chains is reduced to a level that triggers the formation of cross-link bonding. This drastically changes the nature of the covalent bonding in PPTA. In the PPTA polymer chains, the coordination of the backbone atoms varies from one to three. Coordination four may occur when cross-linking is triggered by the bonding between backbones of adjacent molecules. We illustrate the cross-linking process by calculating the change in coordination of

the atoms. Figures 2(f) and 2(g) illustrate a configuration in the cross-linking regime, where the atoms are colored by their coordination number, calculated here as the number of covalent bonds each atom has based on the same pair-wise cutoffs used for hybridization analysis, i.e., C–C 1.7, C–N 1.7, C–O 1.5, and C–H 1.3 Å. We use red, yellow, green, light blue, and dark blue to color four, three, two, one, and zero coordinated atoms, respectively. The presence of four coordinated atoms confirms the formation of cross-linking bonds. This is because in the equilibrated structure, the maximum coordination of an atom is three. For a fourth bond to occur within the same polymer chain, the polymer backbone would need to kink significantly. Since this is not observed, in order for coordination four to occur, an atom must covalently bond with an atom on an adjacent polymer chain, i.e., the polymer chains must cross-link.

We continue by investigating the shock response of PPTA along the [100] direction, probing the stability of the PPTA sheet stacking. Consistent with the previous simulations of shock along the [010] direction, we set the shock velocity in MSST simulations, allowing us to calculate the particle velocity. We set U_s in the range between 4.0 and 10.0 km/s to examine the effect of different shock intensities. From the calculated U_p values from all simulations, we compile the shock Hugoniot curve shown in Fig. 4(a). A combined analysis of the shock Hugoniot data and the changes in the structure of the system indicates two shock response regimes along the

[100] direction: elastic/plastic and cross-linking, which are denoted by solid circles and triangles in Fig. 4(a), respectively.

Along the [100] direction for particle velocities up to $U_p = 2.24$ km/s, an elastic/plastic regime is observed. To characterize the structural changes triggered in this regime, we perform a local analysis of the PPTA chains' conformation and the integrity of the initially flat PPTA sheets in the simulation cells. Figures 4(b) and 4(c) illustrate a simulation cell in the elastic/plastic regime at $U_p = 0.902$ km/s. This regime is characterized by large regions where the PPTA crystal is compressed along the [100] direction while retaining its structure. However, shear bands are generated and propagate diagonally in the system, i.e., at about ~45° with the shock direction. Such shear bands have a thickness spanning about three to four PPTA chains, where the molecules develop a rather planar conformation, in which the angle between phenylene groups becomes close to 0°. The change in molecule conformation is quantified by the change in the dihedral angle between phenylene and amide groups in the PPTA molecules shown in Figs. S2 and S3. This plastic deformation response preserves the hydrogen bonding level to about the same level existing in the thermalized crystal configuration. This hydrogen bond-preserving shock response mechanism along the [100] direction contrasts with the shock response along the [010] direction and indicates a superior shock resilience of [100] aligned PPTA crystals. Additional simulations of shock pressure release demonstrate that the elastic/plastic
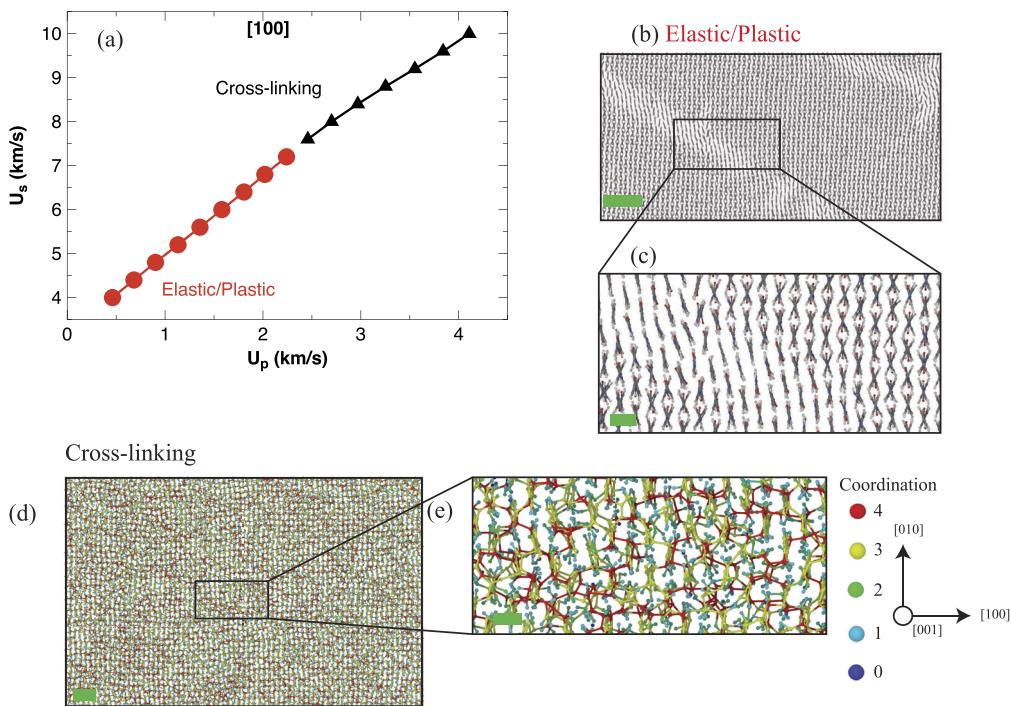

FIG. 4. PPTA [100] shock response regimes. (a) Shock Hugoniot. (b) System at the elastic/planarization shock regime at $U_p = 0.902$ km/s with the (c) zoomed-in region. (d) System at the crosslinking regime for $U_p = 4.11$ km/s with (e) the inset showing increased coordination. (d) and (e) The polymer backbone colored by coordination from 0 (dark blue) to 4 (red). (b) and (c) Colored by atom type based on the scheme given in Fig. 1. Scale bar dimensions: (b) 25 Å, (c) 5 Å, (d) 10 Å, and (e) 2.5 Å. (b)–(e) Produced with OVITO version 5.3.3.
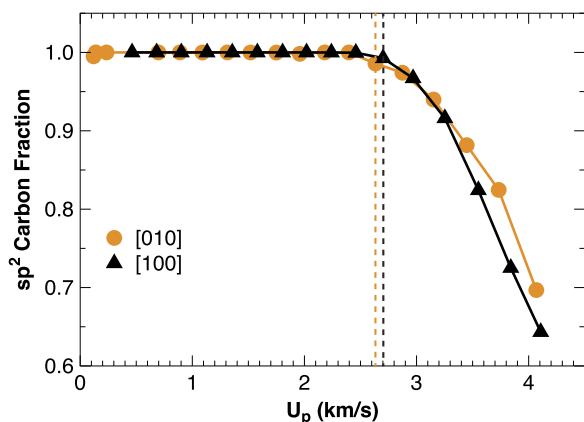
FIG. 5. The fraction of sp^2 carbon as a function of particle velocity.

regime leads to irreversible changes to the structure of the PPTA crystal.

Akin to the shock response along the [010] direction, intense shocks along the [100] direction also trigger cross-linking. For the [100] direction, the cross-linking regime is triggered at U_p = 2.46 km/s. We illustrate this process in Figs. 4(d) and 4(e), where the atoms are colored based on their coordination: red, yellow, green, light blue, and dark blue denoting four, three, two, one, and zero coordination, respectively. Here, again, the existence of four coordinated atoms confirms the presence of cross-linkage. The entire simulation cell is illustrated in Fig. 4(d) and shows a homogeneous cross-linking process. The zoomed-in view of Fig. 4(e) highlights the local configuration of atoms and cross-linking bonds.

To further understand the breakdown of PPTA under intense shock loading, we focus on the changes of bonding configurations of the carbon atoms. Cross-links involving carbon atoms are of particular interest because their aromatic rings are a defining feature of PPTA. An aromatic ring consisting of six sp^2 carbon atoms is a stable structure. Thus, its breakdown in PPTA chains

indicates the loss of stability of the polymer chains with the consequent decomposition of the system. All carbon atoms in a defect-free PPTA structure have coordination three and are found in the sp^2 hybridization. To analyze carbon cross-linking in the system, including the breakdown of aromatic rings, we calculate the evolution of sp^2 carbon fraction as a function of particle velocity, as shown in Fig. 5. The results indicate that shocks of increasing strength along both [010] and [100] directions eventually drive the change in carbon hybridization from sp^2 to sp^3, which implies the formation of cross-links. The hybridization of the carbon atoms is defined by the number of bonds formed, which are calculated based on cutoff radii, i.e., C–C 1.7, C–N 1.7, C–O 1.5, and C–H 1.3 Å. For the transition to sp^3 hybridization to be significant, we consider a reduction of at least 1% in the fraction sp^2 carbon atoms. The hybridization change reaches this threshold at U_p = 2.70 km/s for the [100] direction and U_p = 2.63 km/s for the [010] direction, as indicated by the dashed lines in Fig. 5. The fraction of sp^2 carbon decreases sharply for both directions as the particle velocity is increased and cross-linkage permeates the system. By $U_p \geq$ 4 km/s, more than 30% of the carbon atoms in both orientations display sp^3 hybridization as cross-linking connects PPTA chains across the whole system.

To better understand the changes in the PPTA crystalline structure occurring at shock intensities below the cross-linking threshold, we examine the relative arrangement of the PPTA polymer chains in the shocked states. To accomplish that, we consider the PPTA chains' center of mass, calculated considering its backbone carbon, nitrogen, and oxygen atoms. From the resulting 2D center of mass configurations, we analyze the structural changes occurring in the molecule arrangement under different shock conditions. From the set of center-of-mass points, we calculate the pair distribution function, g(r), shown as solid curves in Fig. 6. Figure 6 shows g(r) of the thermalized crystal configuration at 300 K (black curves), g(r) of the structure compressed along the [100] direction for U_p = 2.24 km/s (red curve), and the amorphous structure generated at U_p = 1.75 km/s for shock along the [010] direction (purple curve). The insets of Fig. 6 show the respective representative arrangements of the center-of-mass configurations for the three cases. The change in g(r) for weak and intermediate shock compression along the [100] direction is shown in Fig. 6(a). One can
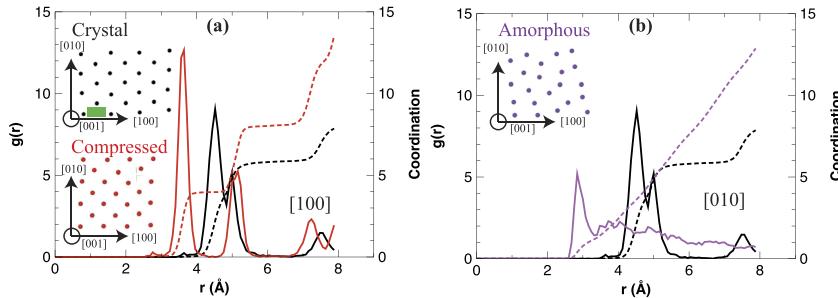

FIG. 6. Pair distribution function (solid curves) and coordination number (dashed curves) of the center of mass of molecules for shocks along (a) [100] and (b) [010] directions. The crystal structure is thermalized at 300 K. The compressed crystal sample is taken from the simulation at U_p = 2.24 km/s along [100]. The amorphous structure sample is taken from the simulation at U_p = 1.75 km/s along [010]. Scale bar dimension: 4 Å. Insets are produced with OVITO version 5.3.3.

note that the linear compression along the [100] direction split the first and second peaks of the relaxed crystal g(r). At the same time, the third peak, corresponding to the distance between the second nearest PPTA sheets, merges with the second peak, corresponding to the distance between PPTA chains in the same sheet; see the inset of Figs. 6(a) and 1(b). The corresponding coordination number changes are highlighted as dashed curves in Fig. 6(a). The compressed structure g(r) first peak displays coordination number 4, while the coordination at the second peak is raised to 8. In contrast, the g(r) curve shown in Fig. 6(b) for shock along the [010] indicates drastic changes in the arrangement of the PPTA chains. The shock compression at U_p = 1.75 km/s shifts the first peak, corresponding to the nearest neighbor distance, from 4.52 to 2.84 Å. The absence of any peaks in g(r) beyond the first peak, and the gradual decrease in the value to ~1, indicates the loss of medium and long-range order in the system. Such g(r), typical of amorphous structures, implies a finite probability of finding a molecule at any distance relative to a given reference molecule. The corresponding coordination number increases smoothly with distance.

IV. DISCUSSION

It is instructive to compare the different shock responses of PPTA presented considering its intrinsic bond hierarchy. The results of the shock response along the [010] and [100] directions in PPTA crystals, as represented in Figs. 2 and 4, display a clear anisotropic response, which is consistent with the contrasting bonding in the crystal along these two directions, i.e., hydrogen bonding along the [010] direction and van der Waals interaction along the [100] direction. The contrasting shock response observed leads to very different shock resilience. The molecular planarization that we observe in the shear bands that form during shocks along the [100] direction preserves the hydrogen bond network, explaining the high shock resilience of PPTA along this direction. In contrast, the early amorphization that occurs during shocks along the [010] direction disrupts the hydrogen bond network, leading to a relatively limited elastic/plastic response. The anisotropic response of PPTA to stress loading is also reported in other studies. For example, ReaxFF atomistic simulations of tensile loading indicate different mechanical properties of PPTA, such as failure strain and ultimate stress, when the loading is applied along the [100], [010], and [001] directions.[41] Shock experiments of Kevlar/epoxy composites also show different shock responses of the material to loading along different directions, i.e., a two shock wave structure is formed when fibers are oriented longitudinally to the shock propagation, while a single wave is generated with a perpendicular orientation of the fibers.[42]

The results of this work directly build on and complement a recent work by Tiwari et al.,[21] where shock on PPTA was investigated by performing MSST ab initio calculations. Consistent with the results presented by Tiwari et al.,[21] this work demonstrates the importance of hydrogen bonds in the anisotropic shock response of PPTA. Akin to their work, the results here indicate three distinct regimes for the shock response along the [010] direction, i.e., an elastic precursor is followed by an amorphization of the structure and finally cross-linking of the polymer chains for increasing shock intensity. In contrast to their work, we observe an elastic/plastic

regime, whereas Tiwari et al. reported a precursor regime composed of pure elastic compression. The coexistence of elastic and plastic regions in a polymer material under shock loading is expected, considering the weak intermolecular forces holding together its crystalline molecular arrangement. While ab initio simulations of Tiwari et al. accurately described the local shock response of PPTA crystals, the small box sizes employed in the simulations may hinder the generation of plastic regions.

Akin to the results of Tiwari et al.,[21] cross-linking is also observed here for high-intensity shocks along the [100] direction. In contrast, our results show no pure elastic regime in response to shock along the [100] direction. Instead, simulations here indicate an elastic/plastic response of the PPTA system in a wide range of particle velocities until the cross-linking process is triggered. However, there are intriguing similarities between the elastic/plastic regime in the present work and the transformation regime reported by Tiwari et al. for shocks along the [100] direction. Both studies indicate the planarization of molecules. In the work of Tiwari et al., the planarization is combined with changes in the PPTA sheet stacking, leading to a transition from orthorhombic to a monoclinic structure. In the current work, the planarization of molecules leads to the formation of shear bands that traverse the whole simulation box, Fig. 4(b). For $U_p \leq 0.902$ km/s, regions with planarized molecules are formed across the sample. For increasing U_p, these regions connect and form a well-defined shear band that traverses the whole system, as can be seen in the supplementary material, Fig. S1. From U_p = 1.36 km/s, we observe smaller isolated bands of planarized molecules distributed throughout the simulation cell. The structural transformation reported by Tiwari et al.[21] may also be a size effect on the simulation results as it requires planarization of all molecules in the simulation cell and a well-defined rearrangement of the PPTA sheet stacking. The simulation results, here, indicate that the formation of shear bands from the local planarization of molecules requires a much larger simulation box since the shear band width spans about three to four PPTA molecules, Fig. 4(c).

An important process in the shock response of PPTA, observed in the present study and in the work of Tiwari et al.,[21] is cross-linking along both the [100] and [010] directions for high shock intensity. This shock-induced generation of new bonds in the form of polymer chain cross-links is similar to the bond formation observed in simulations by Qi and Sinnott when organic molecules were impacted against hydrogen-terminated diamond.[43] Similar shock-induced cross-linking is also reported in reactive MD simulations of poly-dimethylsiloxane.[44] However, cross-linking was absent in shock loading reactive MD simulations of other polymer systems, such as polyvinyl nitrate.[27] Instead, they reported polymer dissociation via chemical reaction and the formation of small molecules such as H_2O at the highest shock intensities studied.[27]

The observation of shear bands for shocks along the [100] direction in the present work adds to the variety of external conditions known to generate the shear bands in PPTA. Experimentally, shear bands are observed in transmission microscope images of aramid fibers that are subjected to compressive stress in fiber bending tests.[12,45] Additionally, reactive force field simulations have shown shear band formation for PPTA cells subjected to tensile stress.[16] The shear band formation mechanisms observed in this work may be the underlying atomistic mechanism of shear band formation in the experimental studies of compression that may be

indicative of the same atomistic mechanism appearing in both fiber bending compression and shock compression.

It is informative to relate the present simulation to experiments of shock loading in aramid fibers, such as PPTA. In many shock loading experiments on Kevlar, a material primarily based on PPTA, the intrinsic shock response of PPTA to a wide set of directions is probed. As a result, the shock response along the [100] and [010] PPTA directions cannot be compared directly with experimental results of shock on Kevlar. However, atomistic deformation mechanisms for the [100] and [010] directions in the present study may be relevant to understanding Kevlar's shock response. For example, an experimental investigation of the shock response of Kevlar/epoxy composites, performed using an explosive driver system, shows two regimes of shock response in the shock Hugoniot, suggesting the presence of a structural phase transition in the Kevlar fibers at elevated pressures.[42] The present work indicates a shock-induced amorphization, for shocks along the [010] direction, which may be linked to this reported phase transition.

V. CONCLUSION

The present work expands on the experimental and simulation studies of the response of polymers to external conditions by shedding light on the shock response of PPTA. We used reactive force field molecular dynamics to further clarify the highly anisotropic shock response of PPTA crystals. Shock loading along the [100] direction leads to the formation of PPTA shear bands, where PPTA chain molecules' phenylene groups become co-planar, preserving the hydrogen bond network. In contrast, shock loading along the [010] direction leads to hydrogen bond scission and the generation of an amorphous structure. These results demonstrate the atomistic grounds for the high shock resilience found in experiments and applications of PPTA and also suggest that processing techniques in which the polymer backbone is in line with the fiber axis and the [100] direction is highly oriented with the anticipated impact direction would further improve the shock resilience of PPTA-based materials.

SUPPLEMENTARY MATERIAL

See the supplementary material for the following: time steps and total simulation time for the shock simulations performed (Table S1); final configuration of simulation cells for shocks along the [100] direction in the elastic/plastic regime (Fig. S1); dihedral angle between phenylene and amide groups in PPTA molecules as a function of particle velocity for shock along the [100] direction in the elastic/plastic regime (Fig. S2); histograms of dihedral angles between phenylene and amide groups in PPTA molecules for shocks applied along the [100] direction (Fig. S3); simulation cells before and after the transition from the elastic/plastic to amorphization regimes for shocks along the [010] direction (Fig. S4); data regarding atoms forming cross-link bonds in the cross-linking regime (Table S2); ReaxFF interatomic potential (description of the reparameterization made to the ReaxFF-lg potential parameters); size effects (ReaxFF simulations on smaller simulation cells; description of size effects on the simulation results; and additional simulation results on small cells); and MSST simulations convergence (plots of particle

velocity and total pressure as a function of simulation time to show the convergence of the MSST shock simulations).

AUTHOR DECLARATIONS

Conflict of Interest

The authors have no conflicts to disclose.

Author Contributions

Emily J. Gurniak: Data curation (equal); Formal analysis (equal); Investigation (equal); Methodology (equal); Validation (equal); Visualization (equal); Writing – original draft (equal). **Subodh C. Tiwari:** Conceptualization (equal); Data curation (equal); Formal analysis (equal); Methodology (equal). **Sungwook Hong:** Data curation (equal); Methodology (equal); Software (equal); Validation (equal). **Aiichiro Nakano:** Conceptualization (equal); Funding acquisition (equal); Project administration (equal); Resources (equal). **Rajiv K. Kalia:** Conceptualization (equal); Funding acquisition (equal); Resources (equal). **Priya Vashishta:** Conceptualization (equal); Funding acquisition (equal); Resources (equal). **Paulo S. Branicio:** Conceptualization (equal); Formal analysis (equal); Project administration (equal); Supervision (equal); Writing – review & editing (equal).

DATA AVAILABILITY

The data that support the findings of this study are available within the article and its supplementary material.

REFERENCES

[1] C. W. Peterson, Sci. Am. **262**, 108 (1990).

[2] W. H. Coleman, D. Chen, Y.-q. Li, A. E. Cowan, and P. Setlow, J. Bacteriol. **189**, 8458 (2007).

[3] J. Mayo and E. Wetzel, Text. Res. J. **84**, 1233 (2014).

[4] V. P. W. Shim, C. T. Lim, and K. J. Foo, Int. J. Impact Eng. **25**, 1 (2001).

[5] M. G. Northolt, P. den Decker, S. J. Picken, J. J. M. Baltussen, and R. Schlatmann, *Polymeric and Inorganic Fibers* (Springer-Verlag, Berlin, Heidelberg, 2005), pp. 1–108.

[6] G. Zhu, W. Goldsmith, and C. K. H. Dharan, Int. J. Solids Struct. **29**, 399 (1992).

[7] J. Nasser, J. Lin, and H. Sodano, J. Appl. Phys. **124**, 045305 (2018).

[8] Y.-J. Pan, C.-T. Hsieh, C.-L. Huang, C.-H. Huang, C.-W. Lou, C.-W. Li, and J.-H. Lin, Fibers Polym. **16**, 2682 (2015).

[9] Y. Rao, A. J. Waddon, and R. J. Farris, Polymer **42**, 5937 (2001).

[10] R. J. Young, D. Lu, R. J. Day, W. F. Knoff, and H. A. Davis, J. Mater. Sci. **27**, 5431 (1992).

[11] J. Liu and P. H. Geil, J. Macromol. Sci., Part B **36**, 61 (1997).

[12] M. G. Dobb, D. J. Johnson, and B. P. Saville, Polymer **22**, 960 (1981).

[13] D. Ahmed, Z. Hongpeng, K. Haijuan, L. Jing, M. Yu, and Y. Muhuo, Mater. Res. **17**, 1180 (2014).

[14] L. Avanzini, L. Brambilla, C. Marano, and A. Milani, Polymer **116**, 133 (2017).

[15] M. Depner and B. L. Schürmann, Polymer **33**, 398 (1992).

[16] S. Chowdhury, S. Sockalingam, and J. Gillespie, Fibers **5**, 7 (2017).

[17] B. Mercer, E. Zywicz, and P. Papadopoulos, Polymer **114**, 329 (2017).

[18] S. Sockalingam, S. C. Chowdhury, J. W. Gillespie, and M. Keefe, Text. Res. J. **87**, 984 (2017).

[19] T. C. O'Connor and M. O. Robbins, ACS Macro Lett. **5**, 263 (2016).

[20] M. Grujicic, P. S. Glomski, B. Pandurangan, W. C. Bell, C.-F. Yen, and B. A. Cheeseman, J. Mater. Sci. **46**, 4787 (2011).

[21] S. C. Tiwari, K. Shimamura, A. Mishra, F. Shimojo, A. Nakano, R. K. Kalia, P. Vashishta, and P. S. Branicio, J. Phys. Chem. B **123**, 9719 (2019).

[22] T. L. Chantawansri, T. W. Sirk, E. F. C. Byrd, J. W. Andzelm, and B. M. Rice, J. Chem. Phys. **137**, 204901 (2012).

[23] J. Lütgert, J. Vorberger, N. J. Hartley, K. Voigt, M. Rödel, A. K. Schuster, A. Benuzzi-Mounaix, S. Brown, T. E. Cowan, E. Cunningham, T. Döppner, R. W. Falcone, L. B. Fletcher, E. Galtier, S. H. Glenzer, A. Laso Garcia, D. O. Gericke, P. A. Heimann, H. J. Lee, E. E. McBride, A. Pelka, I. Prencipe, A. M. Saunders, M. Schölmerich, M. Schörner, P. Sun, T. Vinci, A. Ravasio, and D. Kraus, Sci. Rep. **11**, 12883 (2021).

[24] J. B. Hooper, D. Bedrov, G. D. Smith, B. Hanson, O. Borodin, D. M. Dattelbaum, and E. M. Kober, J. Chem. Phys. **130**, 144904 (2009).

[25] M. G. Fröhlich, T. D. Sewell, and D. L. Thompson, J. Chem. Phys. **140**, 024902 (2014).

[26] A. Neogi and N. Mitra, J. Appl. Phys. **119**, 165903 (2016).

[27] M. M. Islam and A. Strachan, J. Phys. Chem. C **121**, 22452 (2017).

[28] T. R. Mattsson, J. M. D. Lane, K. R. Cochrane, M. P. Desjarlais, A. P. Thompson, F. Pierce, and G. S. Grest, Phys. Rev. B **81**, 054103 (2010).

[29] M. G. Dobb, D. J. Johnson, and B. P. Saville, J. Polym. Sci., Polym. Phys. Ed. **15**, 2201 (1977).

[30] M. Panar, P. Avakian, R. C. Blume, K. H. Gardner, T. D. Gierke, and H. H. Yang, J. Polym. Sci., Polym. Phys. Ed. **21**, 1955 (1983).

[31] M. G. Dobb, D. J. Johnson, and B. P. Saville, J. Polym. Sci.: Polym. Symp. **58**, 237 (2007).

[32] A. P. Thompson, H. M. Aktulga, R. Berger, D. S. Bolintineanu, W. M. Brown, P. S. Crozier, P. J in 't Veld, A. Kohlmeyer, S. G. Moore, T. D. Nguyen, R. Shan, M. J. Stevens, J. Tranchida, C. Trott, and S. J. Plimpton, Comp. Phys. Comm. **271**, 10817 (2022).

[33] M. G. Northolt, Eur. Polym. J. **10**, 799 (1974).

[34] K. Chenoweth, A. C. T. van Duin, and W. A. Goddard, J. Phys. Chem. A **112**, 1040 (2008).

[35] E. J. Reed, L. E. Fried, and J. D. Joannopoulos, Phys. Rev. Lett. **90**, 235503 (2003).

[36] A. Stukowski, Modell. Simul. Mater. Sci. Eng. **18**, 015012 (2010).

[37] S. C. Chowdhury and J. W. Gillespie, Comput. Mater. Sci. **148**, 286 (2018).

[38] E. N. Baker and R. E. Hubbard, Prog. Biophys. Mol. Biol. **44**, 97 (1984).

[39] F. Fabiola, R. Bertram, A. Korostelev, and M. S. Chapman, Protein Sci. **11**, 1415 (2002).

[40] J. Rösler, H. Harders, and M. Bäker, *Mechanical Behaviour of Engineering Materials* (Springer, Berlin, Heidelberg, 2007).

[41] Q. Yang, W. Li, S. T. Stober, A. B. Burns, M. Gopinadhan, and A. Martini, Macromolecules **54**, 8289 (2021).

[42] V. Mochalova, A. Utkin, A. Savinykh, and G. Garkushin, Compos. Struct. **273**, 114309 (2021).

[43] L. Qi and S. B. Sinnott, J. Phys. Chem. B **101**, 6883 (1997).

[44] A. C. T. van Duin, S. V. Zybin, K. Chenoweth, L. Zhang, S. -P. Han, A. Strachan, and W. A. Goddard III, AIP Conf. Proc. **845**, 581–584 (2006).

[45] S. C. Smith, E. K. Lau, and S. Backer, Text. Res. J. **48**, 104 (1978).